

High purity two-dimensional levitated mechanical oscillator

Q. Deplano,^{1,2} A. Pontin,³ A. Ranfagni,¹ F. Marino,^{3,2} and F. Marin^{1,4,2,3,*}

¹*Dipartimento di Fisica e Astronomia, Università di Firenze,
via Sansone 1, I-50019 Sesto Fiorentino (FI), Italy*

²*INFN, Sezione di Firenze, via Sansone 1, I-50019 Sesto Fiorentino (FI), Italy*

³*CNR-INO, largo Enrico Fermi 6, I-50125 Firenze, Italy*

⁴*European Laboratory for Non-Linear Spectroscopy (LENS),
via Carrara 1, I-50019 Sesto Fiorentino (FI), Italy*

In recent years, levitated optomechanics has delivered on the promise of reaching the motional quantum ground state. An important next milestone of the field would be the generation of mechanical entanglement. An ideal candidate is the two-dimensional motion in the polarization plane of an optical tweezer inside an optical cavity, where optical and mechanical modes are coupled via coherent scattering. Necessary conditions towards this achievement are two-dimensional ground state cooling along with substantial spectral overlap between the two modes. The latter condition is required to generate the necessary correlations, but unfortunately, it hinders efficient cooling thus narrowing the useful parameter space. In this work, we report the achievement of a high purity two-dimensional state in a regime where the strong optomechanical coupling induces the desired spectral superposition between oscillations in different directions, as reflected in the non-trivial spectral shape of the detected cavity field. As a result, significant correlations consistently arise between any pair of orthogonal directions, preventing the motion from being reduced to two independent one-dimensional oscillators and leading to higher purity compared to that scenario. Our system serves as an excellent platform for realizing continuous variable entanglement in two-dimensional motion.

Levitated optomechanical systems provide a powerful platform for the manipulation of mesoscopic quantum objects with applications ranging from fundamental physics [1–3] to the quantum sensing [4, 5] and technologies [6]. Some of these systems have been cooled near the zero point energy [7–11] opening the way towards more refined quantum experiments including the preparation of novel quantum states [12–15] and tests of the quantised nature of gravity [16].

The motion of a levitated nanoparticle in the transverse plane of a tightly focused laser beam (optical tweezer [17]) in high vacuum [18, 19] offers a valuable opportunity to realise a two-dimensional oscillator with quantum properties. The optical potential generated by the tweezer light is pro-

* Electronic mail: francesco.marin@unifi.it

portional to its intensity, whose profile has an elliptical shape near the focus. In the transverse plane it is well approximated by a paraboloid that defines two orthogonal axes to which different natural frequencies of the oscillatory motion of the nanoparticle are associated. We will call them X and Y axes. The axis corresponding to the tighter focusing direction (X), providing the highest oscillation frequency, is typically orthogonal to the main polarization axis of the tweezer [20].

By placing the levitated particle inside an optical cavity with a suitable resonance frequency, a mode of the cavity field is populated by the scattered tweezer light. The oscillatory motion of the nanoparticle is coupled to the cavity field via this coherent scattering [21–24]. When the particle is positioned on a node of the cavity standing wave, it is precisely the motion along the cavity axis (*bright mode*) that is coupled to the cavity field [25–27]. Consequently, the X and Y oscillations have optomechanical coupling rates proportional to $\sin \theta$ and $\cos \theta$ respectively, where θ is the angle between the Y direction and the cavity axis, which is assumed to be orthogonal to the tweezer axis. If θ is close to 90° , the X oscillation can be optically cooled very efficiently by red detuning the tweezer light with respect to the cavity resonance. Thermal occupancies below unity [7] (as low as 0.5 [8, 9]) have actually been achieved. On the other hand, an angle θ close to 45° allows to obtain significant optomechanical coupling and cooling for both the X and the Y motion. If the two mechanical resonances remain well separated with respect to their width, which is enhanced by the optomechanical damping, the planar motion can still be considered as the sum of two independent mechanical modes, which could be jointly cooled near [8] and even both below [9] unity occupation number.

If the two eigenfrequencies are close to each other, the full potential of a two dimensional quantum system emerges thanks to the spectral overlap of the X and Y modes. For instance, it enabled the observation of vectorial polaritons [28] and the cancellation of the quantum backaction [29]. On the other hand, two-dimensional cooling becomes more difficult because the motion orthogonal to the cavity axis (*dark mode*) is not directly coupled to the optical field, but it is simply sympathetically cooled by the bright mode [26] with a rate proportional to the difference between the two eigenfrequencies.

In this work, we push the optical cooling of the two-dimensional motion of a levitated nanosphere close to the ground state (i.e., achieving thermal occupancy well below unity in all directions) by going beyond the optomechanical weak-coupling regime. By maintaining significant spectral overlap between the X and Y modes we ensure that they both largely share the same bath, in which quantum fluctuations play a major role.

The resulting correlations are a fundamental characteristic of our two-dimensional dynamics,

which cannot be simply decomposed into the sum of independent orthogonal oscillations.

As an indicator of quantumness, we calculate the state purity. We show that, thanks to the correlation between X and Y , its value is significantly greater than the simple $1/(2n_x + 1)(2n_y + 1)$ attained by separated oscillators having the thermal occupancies n_x and n_y . This makes evident the enhanced quantumness of the system. The motion then exhibits correlations between high purity oscillators, and it thus provides an important step toward the achievement of two-dimensional quantum entanglement.

A 100 nm silica nanosphere is loaded onto an optical tweezer in a first chamber under low vacuum conditions, then transferred to a second tweezer in the science chamber at a pressure of about 10 mbar [30]. The science tweezer is based on 250 mW light power generated by a Nd:YAG NPRO laser at 1064 nm. A doublet of aspheric lenses, with focal lengths of 18.4 mm and 3.1 mm respectively, collects the light from a polarization maintaining fiber and refocuses it with a waist narrower than $1 \mu\text{m}$. This optical system can be positioned with nanometric precision inside an optical cavity whose optical axis is orthogonal (within $\sim 1^\circ$) to the axis of the tweezer. The light is linearly polarized along a direction at $\sim 45^\circ$ with respect to the cavity axis (Fig. 1). The oscillation frequencies of the nanosphere in the optical potential are, respectively, $(\Omega_x, \Omega_y, \Omega_z)/2\pi = (121.1, 108.5, 21.4)$ kHz for the (X, Y, Z) axes.

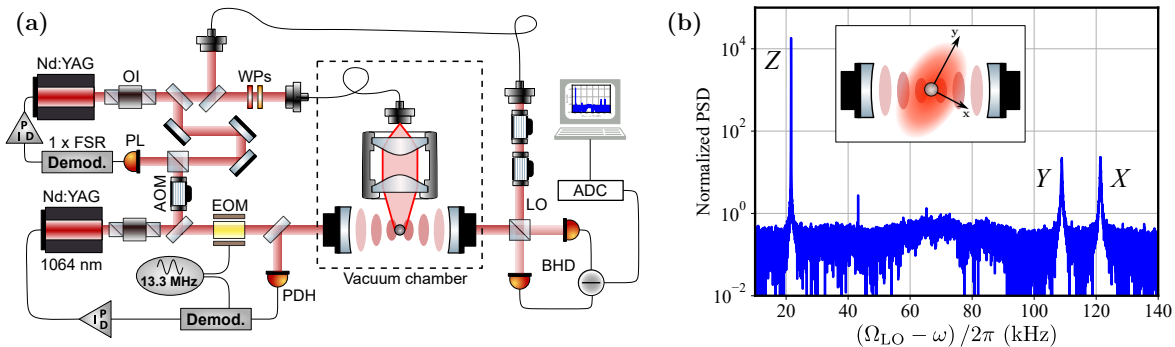


FIG. 1. **Overview of the experiment.** a) Simplified scheme of the experimental setup. OI: optic isolator, WP: wave plate, PL: phase locking photodiode, AOM: acousto-optic modulator, EOM: electro-optic modulator, PDH: Pound-Drever-Hall detection, LO: local oscillator, BHD: balanced heterodyne detection, ADC: analog-to-digital converter. b) Power spectral density (PSD) of the heterodyne signal for a detuning $\Delta/2\pi = -250$ kHz. We show the left (anti-Stokes) sideband, and we report in the abscissa $(\Omega_{LO} - \omega)/2\pi$. The spectrum is normalized to the measured shot noise which is then subtracted (the dark noise, which is ~ 10 dB lower than the shot noise, is preliminarily subtracted from all spectra). The three resonance peaks corresponding to the X , Y and Z modes are identified. The inset shows a scheme a plane orthogonal to the tweezer axis, where Y denotes the tweezer polarization axis, and X its orthogonal direction.

The optical cavity has a linewidth of $\kappa/2\pi = 57$ kHz (full width at half maximum) and it is made with a pair of equal concave mirrors in a nearly concentric configuration, giving a free-spectral-range of $\text{FSR} = 3.07$ GHz. An auxiliary Nd:YAG laser is frequency-locked to the optical cavity, while the tweezer laser is phase-locked to the auxiliary laser with a tunable frequency offset equal to $\text{FSR} + \Delta/2\pi$. This setup precisely determines the detuning Δ of the tweezer radiation from a cavity resonance. The light scattered into the cavity mode and transmitted through the end mirror is analyzed using a balanced heterodyne detection.

After the transfer, the tweezer light is red detuned with respect to a cavity resonance, the nanoparticle is positioned on the cavity axis in correspondence of a node of the standing wave, and the science chamber is pumped down to a pressure of about 3×10^{-8} mbar.

The spectrum of the heterodyne signal, normalized to shot noise, can be written as

$$S_{\text{out}}(\Omega_{\text{LO}} + \omega) = 1 + \eta \kappa |\chi_c(\omega)|^2 g_b^2 S_{x_b x_b}(\omega) \quad (1)$$

where Ω_{LO} is the angular frequency of the local oscillator (in our experiment, we set $\Omega_{\text{LO}}/2\pi = 900$ kHz using two consecutive AOMs, working on opposite orders), η is the overall detection efficiency, and g_b is the optomechanical coupling rate for the motion along the cavity axis. The displacement spectrum $S_{x_b x_b}$ of the bright mode appears filtered by the optical susceptibility $\chi_c(\omega) = [-i(\Delta + \omega) + (\kappa/2)]^{-1}$. It can be written as [31]:

$$S_{x_b x_b}(\omega) = \frac{4}{g_b^2} \frac{g_x^2 \Gamma_x |\chi_x|^2 + g_y^2 \Gamma_y |\chi_y|^2 + |g_x^2 \chi_x + g_y^2 \chi_y|^2 \kappa |\chi_c(-\omega)|^2}{|1 - 2i\chi_c^-(g_x^2 \chi_x + g_y^2 \chi_y)|^2} \quad (2)$$

where we have defined $\chi_c^- = \chi_c(\omega) - \chi_c^*(-\omega)$ and the mechanical susceptibilities are $\chi_j(\omega) = \Omega_j [\Omega_j^2 - \omega^2 - i\gamma_j\omega]^{-1}$ (with $j = x, y$). γ_j , g_j and Γ_j are respectively the rates of gas damping, optomechanical coupling, and decoherence.

In Fig. 1b we display an example of such a spectrum, acquired for a detuning of $\Delta/2\pi = -250$ kHz. The oscillations along the X and Y axes, projected along the cavity axis, produce two clear peaks, broadened and shifted by the optomechanical coupling. With the detuning closer to the mechanical frequencies, both modes are cooled and broadened more effectively, so that their spectra largely overlap. This is clearly visible in the heterodyne spectrum displayed in Fig. 2, which is acquired at a detuning of $\Delta/2\pi = -111$ kHz.

In Fig. 2a we show that the model yielding Eqs. (1-2) well fits the experimental data in a wide frequency range where the heterodyne spectrum is dominated by the motion in the $X - Y$ plane. Outside this region, the narrow peak given by the much warmer Z motion is clearly visible around 21 kHz, as well as broader structures due to erratic frequencies of the rotational motion [32, 33].

$\Omega_x/2\pi$ (Hz)	$\Omega_y/2\pi$ (Hz)	$g_x/2\pi$ (Hz)	$g_y/2\pi$ (Hz)	$\Gamma_x/2\pi$ (Hz)	$\Gamma_y/2\pi$ (Hz)
122170 ± 120	109370 ± 150	14130 ± 220	10370 ± 160	$4030 \pm 200 \pm 120$	$3050 \pm 170 \pm 90$

TABLE I. Parameters extracted from the fit of the heterodyne spectrum (left sideband) with the model of Eqs. (1-2). The reported uncertainty is the spread (one standard deviation) on five independent acquisitions. For the decoherence rate, the second quoted error is due to an uncertainty of 5% in the detection efficiency, whose independent measurement yields $\eta = 0.32$.

The theoretical curve fitted to the left (anti-Stokes) sideband well reproduces also the weaker right sideband. This confirms the validity of the independently measured parameters, in particular the detection efficiency η which plays a crucial role in our evaluation of the decoherence rates and consequently of the thermal occupancies.

In the numerator of Eq. (2), we can identify the contributions of the classical noise sources acting on the X and Y oscillators, quantified by the decoherence rates Γ_j , and of the quantum bath provided by the optical vacuum noise. In Figs. 2b-c we highlight that all three noise sources yield relevant and distinct contributions to the spectral shape. It is therefore clear that measuring the projection on the cavity axis is sufficient to fully characterize the two-dimensional motion. Its relevant parameters, deduced from the fit, are reported in Table I.

We remark that the spectral contributions due to classical noise are frequency symmetric in S_{x_b, x_b} , and they differ in the two sidebands of S_{out} only due to the cavity filtering. On the contrary, the quantum noise is present almost exclusively in the Stokes motional sideband where, in our experiment, it largely overwhelms classical noise. This produces markedly different shapes in the two sidebands, a feature that is a clear signature of quantum two-dimensional motion [29] and testifies the low effective temperature achieved.

The quantum steady state of the optomechanical system is characterized by its covariance matrix $V_{ij} = 0.5\langle\{u_i, u_j\}\rangle$ where $u^T = (Q, P, x, p_x, y, p_y)$, P and Q are the two quadratures of the intracavity field, x and y are the positions and p_x and p_y the momenta of the X and Y oscillators normalized to the respective zero-point fluctuations. The covariance matrix can be calculated using

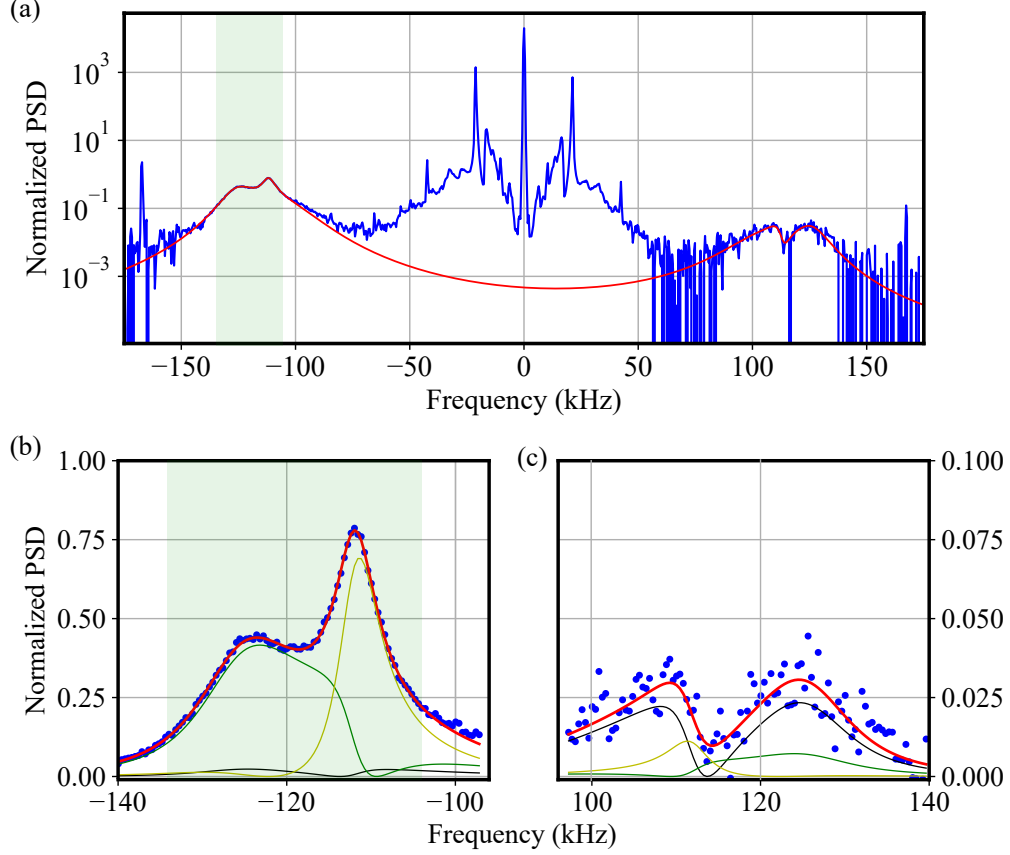


FIG. 2. **Power Spectral Density of the heterodyne signal.** The spectrum is normalized to the measured shot noise which is then subtracted (the dark noise is preliminarily subtracted from all spectra). The abscissa is the frequency difference with respect to the local oscillator. The detuning is $\Delta/2\pi = -111$ kHz. The red solid line shows the fit of Eqs. (1-2) to the experimental left sideband (the spectral region used for the fit is shaded). The lower panels display enlarged views of the left (b) and right (c) sidebands, where different contributions to the fitted curves are shown in dark green (term $\propto \Gamma_x$), yellow (term $\propto \Gamma_y$), and black (quantum noise, term proportional to κ).

the Lyapunov equation $AV + VA^T = -D$ with the drift matrix

$$A = \begin{pmatrix} -\kappa/2 & -\Delta & 0 & 0 & 0 & 0 \\ \Delta & -\kappa/2 & 2g_x & 0 & 2g_y & 0 \\ 0 & 0 & 0 & \Omega_x & 0 & 0 \\ 2g_x & 0 & -\Omega_x & -\gamma_x & 0 & 0 \\ 0 & 0 & 0 & 0 & 0 & \Omega_y \\ 2g_y & 0 & 0 & 0 & -\Omega_y & -\gamma_y \end{pmatrix} \quad (3)$$

and the diffusion matrix $D = \text{Diag}[\kappa, \kappa, 0, 4\Gamma_x, 0, 4\Gamma_y]$. In particular, the two-dimensional motion is described by the covariance matrix of the mechanical system V^M , formed by the last four rows

and columns of V .

The covariance matrix V^M calculated for our system, with the parameters of Table I, is the following

$$V^M = \begin{pmatrix} 2.13 & 0 & -0.32 & -0.59 \\ 0 & 2.07 & 0.52 & -0.34 \\ -0.32 & 0.52 & 2.47 & 0 \\ -0.59 & -0.34 & 0 & 2.48 \end{pmatrix}. \quad (4)$$

The thermal occupancy n_x of the X mode, considered as a one-dimensional oscillator, is given by $(2n_x + 1) = \sqrt{\langle x^2 \rangle \langle p_x^2 \rangle}$ [27], and an equivalent relation holds for the Y mode. Therefore, the diagonal of V^M allows us to infer the steady state occupancies of both modes. Considering the error propagation from the fitted parameters, we derive $n_x = 0.55 \pm 0.06$ and $n_y = 0.74 \pm 0.08$. Both figures are well below unity, a threshold traditionally considered in optomechanics, indicating that the ground state is occupied with probability exceeding 50%.

However, the two thermal occupancies are not sufficient to characterize the two-dimensional motion. The 2x2 off-diagonal blocks of the covariance matrix V^M , containing the correlation terms between the two oscillators, are indeed relevant in our system. A more appropriate parameter for quantifying the quantum character of the two-dimensional state is its purity, defined as $\mu = \text{Tr}(\hat{\rho}^2)$ where $\hat{\rho}$ is the density matrix representing the state. It can be evaluated as the inverse square root of the determinant of the covariance matrix V^M [27, 34]. For our system, we obtain $\mu = 0.209^{+0.026}_{-0.024}$, higher than the value of $1/(2n_x + 1)(2n_y + 1) = 0.192$ that would have been derived in the case of independent oscillators with the same thermal occupancy.

In the weak coupling, resolved sidebands regime, the optically induced width of a mechanical mode is $4g^2/\kappa$. We can quantify the spectral overlap between the X and Y modes using the ratio of their frequency splitting $\delta = (\Omega_x - \Omega_y)$ to their mean width, defining an overlap parameter as $s = 2(g_x^2 + g_y^2)/\kappa\delta$. For $s \ll 1$ the two-dimensional system can be approximately described as the combination of two independent oscillators, while for $s \geq 1$ the full two-dimensional dynamics emerges, and the correlation between the two orthogonal directions becomes significant. To summarize the information on both the state purity and the spectral overlap, we show in Fig. 3 the plot of the (μ, s) parameter space, where we compare our system with the previous results reported in the literature.

The description based on the original, uncoupled X and Y modes does not capture the full physical properties of the optomechanical system. As δ decreases, the motion is better understood using a description based the geometrical bright and dark modes, corresponding to directions

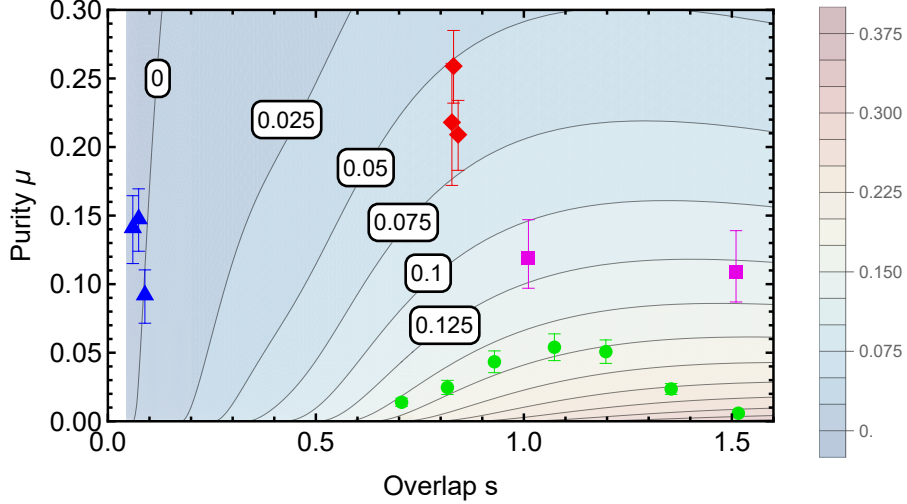


FIG. 3. **Two-dimensional state purity μ for the motion of a nanoparticle in the tweezer transverse plane.** We show the results obtained in different experiments, as a function of the overlap parameter $s = 2(g_x^2 + g_y^2)/\kappa\delta$. Green dots: Ref. [8]. Magenta squares: Ref. [29]. Blue triangles: Ref. [9]. Red diamonds: this work, including the additional data sets [31]. In order to provide an indication of the two-dimensional correlations present in the mechanical system, we also show the contour plot of the minimum c , defined in the main text, calculated with the following parameters: $g_x/2\pi = g_y/2\pi = 12400$ Hz, $\Gamma_x/2\pi = \Gamma_y/2\pi$ varying between 100 Hz and 300 kHz. The other parameters are chosen similar to those of the present work for $s > 0.7$, while for $s < 0.7$ they change to keep realistic ranges. In details, for $s > 0.7$ we use $\kappa/2\pi = 57$ kHz and $(\Omega_x + \Omega_y)/4\pi = 116$ kHz, for $s < 0.7$ both the cavity width and the mean oscillation frequency increase, reaching $\kappa/2\pi = 330$ kHz and $(\Omega_x + \Omega_y)/4\pi = 246$ kHz when $s = 0.07$, approaching the parameters of [9].

parallel and orthogonal to the cavity axis respectively. With this basis, it has been shown that the two-dimensional cooling becomes less effective since the dark mode is not directly coupled to the optical field. Moreover, approaching strong optomechanical coupling, optical cooling becomes less efficient as it assumes a sub-linear dependence on g^2 . As an additional effect of strong coupling, identifying two orthogonal oscillation directions as approximate eigenvectors of the complete optomechanical system becomes poorly accurate [28]. We derive two considerations. First, simultaneously achieving a low effective temperature (i.e., high state purity) and large spectral overlap (i.e., strongly two-dimensional characteristics) is not obvious and requires a proper trade-off in the system parameters. Second, for a fair description of the system we have to abandon the $(X - Y)$ coordinate system, and prioritize indicators that are independent of any specific reference frame.

In order to provide a meaningful estimate of the intrinsic, unavoidable two-dimensional me-

chanical correlations, we have removed the normalization to the zero-point fluctuations of the X and Y modes, avoiding in particular to rely on their uncoupled resonance frequencies $\Omega_{x,y}$, and we have calculated the covariance matrix of the mechanical system in an arbitrary reference frame as $V_\phi^M = R(\phi)NV^MNR^T(\phi)$. Here $R(\phi)$ performs the rotation by an angle ϕ around the axis Z , and $N = \text{Diag}[1/\sqrt{\Omega_x}, \sqrt{\Omega_x}, 1/\sqrt{\Omega_y}, \sqrt{\Omega_y}]$. By writing V_ϕ^M using 2x2 blocks α , β and γ in the form

$$V_\phi^M = \begin{pmatrix} \alpha & \gamma \\ \gamma^T & \beta \end{pmatrix}$$

the correlations between the orthogonal modes of the rotated reference frame are contained in the off-diagonal block γ . We quantify their relevance by the dimensionless parameter $c = \text{Det}[\gamma]/\sqrt{\text{Det}[\alpha]\text{Det}[\beta]}$. Finally, to evaluate the unavoidable two-dimensional correlations we have minimized c with respect to ϕ . A contour plot of the minimum c is provided in Fig. 3, showing that, as expected, larger correlations are present for an overlap parameter around unity.

In conclusion, we have achieved two-dimensional motion of a nanosphere in an optical potential where not only the oscillations predominantly occupy the quantum ground state in all directions across the plane, setting a new benchmark for the purity of the two-dimensional state, but also significant correlations are consistently present between any pair of orthogonal directions. Therefore, the system behavior cannot be reduced to a simple decomposition into two one-dimensional modes. Instead, the motion exhibits distinct two-dimensional characteristics that can be detected spectrally.

The measured correlations are not yet strong enough to produce entanglement between mechanical modes (i.e., between oscillations along two directions of the plane). In fact, it has been shown theoretically that achieving this type of entanglement is almost impossible in a system like ours, where the background is at room temperature and only a single mode of the electromagnetic field is present [35, 36]. However, the system we have developed, characterized by high purity and strong spectral correlations, represents an excellent starting point for achieving entanglement, for example by introducing additional electromagnetic fields [37, 38]. The realization of mechanical entanglement would mark a significant milestone in the development of innovative quantum information schemes [39], as well as for the study of quantum decoherence at the macroscopic level [40–42].

We acknowledge financial support from PNRR MUR Project No. PE0000023-NQSTI and by the European Commission-EU under the Infrastructure I-PHOQS “Integrated Infrastructure Initiative

- [1] T. Li, S. Kheifets, D. Medellin, and M. G. Raizen, Measurement of the instantaneous velocity of a brownian particle, *Science* **328**, 1673–1675 (2010).
- [2] G. Afek, D. Carney, and D. C. Moore, Coherent scattering of low mass dark matter from optically trapped sensors, *Phys. Rev. Lett.* **128**, 101301 (2022).
- [3] D. C. Moore, A. D. Rider, and G. Gratta, Search for millicharged particles using optically levitated microspheres, *Phys. Rev. Lett.* **113**, 251801 (2014).
- [4] A. A. Geraci, S. B. Papp, and J. Kitching, Short-range force detection using optically cooled levitated microspheres, *Phys. Rev. Lett.* **105**, 101101 (2010).
- [5] J. M. H. Gosling, A. Pontin, J. H. Iacoponi, P. F. Barker, and T. S. Monteiro, Sensing directional noise baths in levitated optomechanics, *Phys. Rev. Res.* **6**, 013129 (2024).
- [6] F. Ahrens, W. Ji, D. Budker, C. Timberlake, H. Ulbricht, and A. Vinante, Levitated ferromagnetic magnetometer with energy resolution well below \hbar (2024).
- [7] U. Delić, M. Reisenbauer, K. Dare, D. Grass, V. Vuletić, N. Kiesel, and M. Aspelmeyer, Cooling of a levitated nanoparticle to the motional quantum ground state, *Science* **367**, 892 (2020), <https://science.sciencemag.org/content/367/6480/892.full.pdf>.
- [8] A. Ranfagni, K. Børkje, F. Marino, and F. Marin, Two-dimensional quantum motion of a levitated nanosphere, *Phys. Rev. Research* **4**, 033051 (2022).
- [9] J. Piotrowski, D. Windey, J. Vijayan, C. Gonzalez-Ballester, A. de los Ríos Sommer, N. Meyer, R. Quidant, O. Romero-Isart, R. Reimann, and L. Novotny, Simultaneous ground-state cooling of two mechanical modes of a levitated nanoparticle, *Nature Physics* **19**, 1009 (2023).
- [10] L. Magrini, P. Rosenzweig, C. Bach, A. Deutschmann-Olek, S. G. Hofer, S. Hong, N. Kiesel, A. Kugi, and M. Aspelmeyer, Real-time optimal quantum control of mechanical motion at room temperature, *Nature* **595**, 373 (2021).
- [11] F. Tebbenjohanns, M. L. Mattana, M. Rossi, M. Frimmer, and L. Novotny, Quantum control of a nanoparticle optically levitated in cryogenic free space, *Nature* **595**, 378 (2021).
- [12] M. Roda-Llordes, A. Riera-Campeny, D. Candoli, P. T. Grochowski, and O. Romero-Isart, Macroscopic quantum superpositions via dynamics in a wide double-well potential, *Phys. Rev. Lett.* **132**, 023601 (2024).
- [13] L. Neumeier, M. A. Ciampini, O. Romero-Isart, M. Aspelmeyer, and N. Kiesel, Fast quantum interference of a nanoparticle via optical potential control, *Proceedings of the National Academy of Sciences* **121**, 10.1073/pnas.2306953121 (2024).
- [14] D. S. Bykov, L. Dania, F. Goschin, and T. E. Northup, A nanoparticle stored with an atomic ion in a linear paul trap, arxiv 10.48550/ARXIV.2403.02034 (2024).

- [15] E. Bonvin, L. Devaud, M. Rossi, A. Militaru, L. Dania, D. S. Bykov, O. Romero-Isart, T. E. Northup, L. Novotny, and M. Frimmer, State expansion of a levitated nanoparticle in a dark harmonic potential, *Phys. Rev. Lett.* **132**, 253602 (2024).
- [16] S. Bose, A. Mazumdar, G. W. Morley, H. Ulbricht, M. Toroš, M. Paternostro, A. A. Geraci, P. F. Barker, M. S. Kim, and G. Milburn, Spin entanglement witness for quantum gravity, *Phys. Rev. Lett.* **119**, 240401 (2017).
- [17] A. Ashkin, Acceleration and trapping of particles by radiation pressure, *Phys. Rev. Lett.* **24**, 156 (1970).
- [18] J. Millen, T. S. Monteiro, R. Pettit, and A. N. Vamivakas, Optomechanics with levitated particles, *Reports on Progress in Physics* **83**, 026401 (2020).
- [19] C. Gonzalez-Ballester, M. Aspelmeyer, L. Novotny, R. Quidant, and O. Romero-Isart, Levitodynamics: Levitation and control of microscopic objects in vacuum, *Science* **374**, eabg3027 (2021), <https://www.science.org/doi/pdf/10.1126/science.abg3027>.
- [20] L. Novotny and B. Hecht, *Principles of Nano-Optics*, 2nd ed. (Cambridge University Press, 2012).
- [21] V. Vuletić and S. Chu, Laser cooling of atoms, ions, or molecules by coherent scattering, *Phys. Rev. Lett.* **84**, 3787 (2000).
- [22] D. Windey, C. Gonzalez-Ballester, P. Maurer, L. Novotny, O. Romero-Isart, and R. Reimann, Cavity-based 3d cooling of a levitated nanoparticle via coherent scattering, *Phys. Rev. Lett.* **122**, 123601 (2019).
- [23] U. Delić, M. Reisenbauer, D. Grass, N. Kiesel, V. Vuletic, and M. Aspelmeyer, Cavity cooling of a levitated nanosphere by coherent scattering, *Physical Review Letters* **122**, 123602 (2019).
- [24] A. de los Ríos Sommer, N. Meyer, and R. Quidant, Strong optomechanical coupling at room temperature by coherent scattering, *Nature Communications* **12**, 276 (2021).
- [25] M. Toroš and T. S. Monteiro, Quantum sensing and cooling in three-dimensional levitated cavity optomechanics, *Phys. Rev. Research* **2**, 023228 (2020).
- [26] M. Toroš, U. c. v. Delić, F. Hales, and T. S. Monteiro, Coherent-scattering two-dimensional cooling in levitated cavity optomechanics, *Phys. Rev. Research* **3**, 023071 (2021).
- [27] K. Børkje and F. Marin, Quantum state purity versus average phonon number for characterization of mechanical oscillators in cavity optomechanics, *Phys. Rev. A* **107**, 013502 (2023).
- [28] A. Ranfagni, P. Vezio, M. Calamai, A. Chowdhury, F. Marino, and F. Marin, Vectorial polaritons in the quantum motion of a levitated nanosphere, *Nature Physics* **17**, 1120 (2021).
- [29] A. Ranfagni, F. Marino, and F. Marin, Spectral analysis of quantum field fluctuations in a strongly coupled optomechanical system, *Phys. Rev. Lett.* **130**, 193601 (2023).
- [30] M. Calamai, A. Ranfagni, and F. Marin, Transfer of a levitating nanoparticle between optical tweezers, *AIP Advances* **11**, 025246 (2021), <https://doi.org/10.1063/5.0024432>.
- [31] See supplemental material for details of the calculation and the description of additional data sets.
- [32] A. Pontin, H. Fu, M. Toroš, T. S. Monteiro, and P. F. Barker, Simultaneous cavity cooling of all six degrees of freedom of a levitated nanoparticle, *Nature Physics* **19**, 1003–1008 (2023).

- [33] M. Rashid, M. Toroš, A. Setter, and H. Ulbricht, Precession motion in levitated optomechanics, *Phys. Rev. Lett.* **121**, 253601 (2018).
- [34] A. Serafini, F. Illuminati, and S. D. Siena, Symplectic invariants, entropic measures and correlations of gaussian states, *Journal of Physics B: Atomic, Molecular and Optical Physics* **37**, L21 (2003).
- [35] D. Vitali, S. Mancini, and P. Tombesi, Stationary entanglement between two movable mirrors in a classically driven fabry–perot cavity, *Journal of Physics A: Mathematical and Theoretical* **40**, 8055 (2007).
- [36] C. Genes, D. Vitali, and P. Tombesi, Simultaneous cooling and entanglement of mechanical modes of a micromirror in an optical cavity, *New Journal of Physics* **10**, 095009 (2008).
- [37] M. J. Hartmann and M. B. Plenio, Steady state entanglement in the mechanical vibrations of two dielectric membranes, *Phys. Rev. Lett.* **101**, 200503 (2008).
- [38] J. Li, I. M. Haghghi, N. Malossi, S. Zippilli, and D. Vitali, Generation and detection of large and robust entanglement between two different mechanical resonators in cavity optomechanics, *New Journal of Physics* **17**, 103037 (2015).
- [39] C. Weedbrook, S. Pirandola, R. García-Patrón, N. J. Cerf, T. C. Ralph, J. H. Shapiro, and S. Lloyd, Gaussian quantum information, *Rev. Mod. Phys.* **84**, 621 (2012).
- [40] W. Marshall, C. Simon, R. Penrose, and D. Bouwmeester, Towards quantum superpositions of a mirror, *Phys. Rev. Lett.* **91**, 130401 (2003).
- [41] A. Bassi, K. Lochan, S. Satin, T. P. Singh, and H. Ulbricht, Models of wave-function collapse, underlying theories, and experimental tests, *Rev. Mod. Phys.* **85**, 471 (2013).
- [42] G. Gasbarri, A. Belenchia, M. Carlesso, S. Donadi, A. Bassi, R. Kaltenbaek, M. Paternostro, and H. Ulbricht, Testing the foundation of quantum physics in space via interferometric and non-interferometric experiments with mesoscopic nanoparticles, *Communications Physics* **4**, 155 (2021).

SUPPLEMENTAL MATERIAL

Model

The motion in the transverse tweezer plane is described in terms of dimensionless position and momentum operators x, p_x, y, p_y obtained by normalizing the corresponding physical variables to their respective zero-point fluctuations $x_{\text{zpf}} = \sqrt{\hbar/2m\Omega_{x,y}}$ and $p_{\text{zpf}} = \sqrt{\hbar m\Omega_{x,y}/2}$ (m is the mass of the nanosphere, $\Omega_{x,y}$ the oscillation frequencies of the X and Y modes in the absence of optomechanical interaction). The Langevin equations of motion are:

$$\dot{x} = \Omega_x p_x \tag{5}$$

$$\dot{p}_x = -\Omega_x x - \gamma_x p_x + 2g_x Q + 2\sqrt{\Gamma_x} \xi_x \tag{6}$$

$$\dot{y} = \Omega_y p_y \tag{7}$$

$$\dot{p}_y = -\Omega_y y - \gamma_y p_y + 2g_y Q + 2\sqrt{\Gamma_y} \xi_y \tag{8}$$

$$\dot{Q} = -\Delta P - \frac{\kappa}{2} Q + \sqrt{\kappa} Q_{\text{in}} \tag{9}$$

$$\dot{P} = \Delta Q - \frac{\kappa}{2} P + 2g_x x + 2g_y y + \sqrt{\kappa} P_{\text{in}} \tag{10}$$

where $Q = (a + a^\dagger)$ and $P = i(a^\dagger - a)$ are the quadratures of the intracavity field a , and $Q_{\text{in}} = (a_{\text{in}} + a_{\text{in}}^\dagger)$, $P_{\text{in}} = i(a_{\text{in}}^\dagger - a_{\text{in}})$ are the quadratures of the input vacuum noise. The noise sources have non-null correlation functions $\langle \xi_x(t) \xi_x(t') \rangle = \langle \xi_y(t) \xi_y(t') \rangle = \langle a_{\text{in}}(t) a_{\text{in}}^\dagger(t') \rangle = \delta(t - t')$ (due to the high background temperature, we can classically model the mechanical noise).

The gas damping rates γ_j play a negligible role at low pressure, where optomechanical damping largely dominates, and we fix them at the nominal value of 10^{-4} s^{-1} . The decoherence of the motion is mainly due to collisions with the background gas, and to quantum noise in the dipole scattered light. The corresponding rates $\Gamma_{x,y}$ are left as free parameters in the analysis of the experimental data, and the inferred values well agree, within their uncertainties, with their theoretical estimates [8]. In particular, for this experiment such agreement is obtained by assuming a background pressure in the range $(2 \div 3) \times 10^{-8} \text{ mbar}$, which is indeed the indication given by two pressure gauges in different positions of the vacuum chamber. The optomechanical coupling rates g_x and g_y are proportional to $\sin^2 \theta$ and $\sin \theta \cos \theta$ respectively. Also in this case, we consider them as free parameters in the data analysis, the agreement with the expected values is good [8], and from their ratio we deduce the actual angle of the polarization axis.

From the Langevin equations (5 - 10) we derive the drift and diffusion matrices used in the main text for the Lyapunov equation.

The Langevin equations can be written in the Fourier space as

$$\tilde{Q}(\omega) = i\chi_c^-(\omega) [g_x \tilde{x}(\omega) + g_y \tilde{y}(\omega)] + \tilde{Q}_{\text{in}}(\omega) \quad (11)$$

$$\tilde{x}(\omega) = 2g_x \chi_x(\omega) \tilde{Q}(\omega) + \tilde{N}_x(\omega) \quad (12)$$

$$\tilde{y}(\omega) = 2g_y \chi_y(\omega) \tilde{Q}(\omega) + \tilde{N}_y(\omega) \quad (13)$$

where the tilde denotes Fourier transformed (FT) operators $\tilde{O}(\omega) = \text{FT} [\hat{O}(t)]$, and $\tilde{O}^\dagger(\omega) = \text{FT} [\hat{O}^\dagger(t)]$. We have defined the susceptibilities

$$\chi_j(\omega) = \frac{\Omega_j}{\Omega_j^2 - \omega^2 - i\omega\gamma_j} \quad (14)$$

$$\chi_c(\omega) = \frac{1}{-i(\Delta + \omega) + \kappa/2} \quad (15)$$

with $j = (x, y)$, and the compact form $\chi_c^-(\omega) = \chi_c(\omega) - \chi_c^*(-\omega)$. The noise input terms can be written as

$$\tilde{Q}_{\text{in}}(\omega) = \sqrt{\kappa} \left[\chi_c(\omega) \tilde{a}_{\text{in}}(\omega) + \chi_c^*(-\omega) \tilde{a}_{\text{in}}^\dagger(\omega) \right] \quad (16)$$

$$\tilde{N}_i(\omega) = 2\sqrt{\Gamma_i} \chi_i(\omega) \tilde{\xi}_i. \quad (17)$$

We define the bright mode as $x_b = \frac{1}{g_b} (g_x x + g_y y)$. Using it in Eq. (11) and combining Eqs. (12-13) we obtain two equations respectively for \tilde{Q} and \tilde{x}_b . Inserting the first into the second we derive

$$\tilde{x}_b(\omega) = \frac{2(g_x^2 \chi_x + g_y^2 \chi_y) \tilde{Q}_{\text{in}}(\omega) + g_x \tilde{N}_x(\omega) + g_y \tilde{N}_y(\omega)}{g_b [1 - 2i\chi_c^-(\omega) (g_x^2 \chi_x + g_y^2 \chi_y)]} \quad (18)$$

from which we calculate the displacement noise spectrum

$$S_{x_b x_b}(\omega) = \frac{4}{g_b^2} \frac{g_x^2 \Gamma_x |\chi_x|^2 + g_y^2 \Gamma_y |\chi_y|^2 + |g_x^2 \chi_x + g_y^2 \chi_y|^2 \kappa |\chi_c(-\omega)|^2}{|1 - 2i\chi_c^-(\omega) (g_x^2 \chi_x + g_y^2 \chi_y)|^2} \quad (19)$$

used in the main text.

The cavity output field is given by the input-output relation $a_{\text{out}} = \sqrt{\kappa} a - a_{\text{in}}$, and the heterodyne spectrum normalized to shot noise can be written as

$$S_{\text{out}}(\Omega_{\text{LO}} + \omega) = 1 + \eta \kappa |\chi_c(\omega)|^2 g_b^2 S_{x_b x_b}(\omega). \quad (20)$$

The parameter g_b plays no meaningful role in the model, and indeed it cancels out in the expression of the heterodyne spectrum. We note however that, by defining it as

$$g_b = \sqrt{\frac{g_x^2 \Omega_x + g_y^2 \Omega_y}{\Omega_b}} \quad (21)$$

where

$$\Omega_b = \sqrt{\frac{g_x^2 \Omega_x^3 + g_y^2 \Omega_y^3}{g_x^2 \Omega_x + g_y^2 \Omega_y}} \quad (22)$$

and assuming that $g_x \propto \sin^2 \theta$ and $g_y \propto \sin \theta \cos \theta$, x_b can be identified as the motion along the cavity axis, normalized to the zero-point fluctuations $\sqrt{\hbar/2m\Omega_b}$.

Additional data set

Thanks to a couple of ring electrodes positioned on the tweezer optics at about 1 mm from the nanosphere, we can generate a static electric field along the tweezer axis. Since the nanosphere is in general charged, this allows us to displace its equilibrium position. In this way we slightly tune the oscillation frequencies and, compensating for the tweezer radiation pressure, maximize the frequency splitting between X and Y .

We acquired two additional data sets, at different applied voltages. Unfortunately, in these data sets the signals given by the rotational motion are more evident, and we had to post-select the time series in order to delete the time intervals in which the erratic rotational peaks cross the spectral regions of interest. The overall signal-to-noise ratio is therefore lower than in the spectra described in the main text.

An example is shown in Fig. 4. In panel (c) of the figure, which displays an enlarged view of the right sideband, we also report, together with the theoretical curve fitted to the left sideband, the same theoretical signal with $S_{x_b, x_b}(\omega) \rightarrow S_{x_b, x_b}(-\omega)$. It shows how the heterodyne signal would appear in the case of a mechanical system dominated by classical noise, i.e., when the displacement noise spectrum is frequency symmetric and the difference between the two motional sidebands is due exclusively to the cavity filtering. The huge difference, both in amplitude and shape, compared to the actual spectral signal is a further evidence of the highly quantum nature of the two-dimensional oscillator.

In Table II we summarize the fitted parameters for all data sets (including the first one, discussed in the main text), and in Table III we report the extracted values of thermal occupancy and two-dimensional state purity.

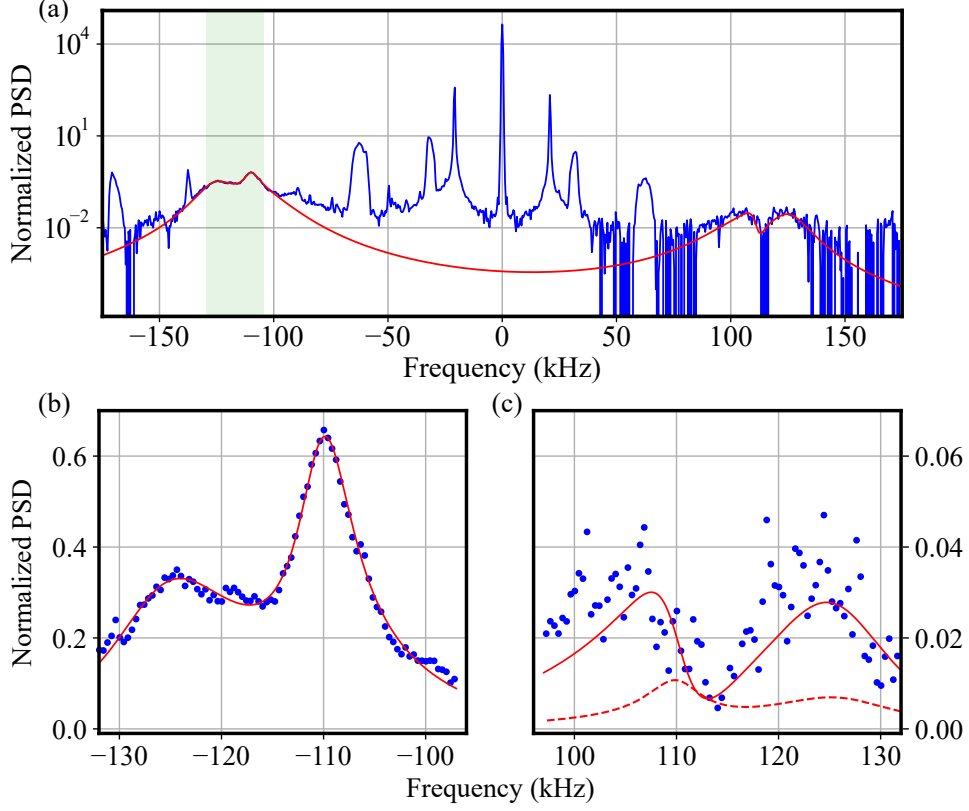


FIG. 4. **Power Spectral Density of the heterodyne signal for an additional data set.** The spectrum is normalized to the measured shot noise which is then subtracted (the dark noise is preliminarily subtracted from all spectra). The abscissa is the frequency difference with respect to the local oscillator. The detuning is $\Delta/2\pi = -110$ kHz, and a voltage of 35 V is applied to the electrodes on the tweezer. The red solid line shows the fit of Eqs. (1-2) to the experimental left sideband (the spectral region used for the fit is shaded). The lower panels display enlarged views of the left (b) and right (c) sidebands. The dashed red line in panel (c) is obtained by replacing $S_{x_b, x_b}(\omega) \rightarrow S_{x_b, x_b}(-\omega)$.

Voltage (V)	0	22.5	35
$\Omega_x/2\pi$ (Hz)	122170 ± 120	122290 ± 280	121610 ± 160
$\Omega_y/2\pi$ (Hz)	109370 ± 150	108970 ± 220	107640 ± 150
$g_x/2\pi$ (Hz)	14130 ± 220	14420 ± 230	15160 ± 310
$g_y/2\pi$ (Hz)	10370 ± 160	10300 ± 190	10060 ± 110
$\Gamma_x/2\pi$ (Hz)	$4030 \pm 200 \pm 120$	$3890 \pm 220 \pm 150$	$3250 \pm 180 \pm 100$
$\Gamma_y/2\pi$ (Hz)	$3050 \pm 170 \pm 90$	$2990 \pm 160 \pm 70$	$2520 \pm 140 \pm 70$

TABLE II. Parameters extracted from the fit of three data sets with the model of Eqs. (1-2). The reported uncertainty is the spread (one standard deviation) on five independent acquisitions. For the decoherence rate, the second quoted error derives from a spread of 5% in the detection efficiency, which is a conservative estimate of the uncertainty of an independent measurement yielding $\eta = 0.32$.

Voltage (V)	0	22.5	35
n_x	$0.553 \pm 0.029 \pm 0.027$	$0.516 \pm 0.027 \pm 0.031$	$0.409 \pm 0.022^{+0.022}_{-0.026}$
n_y	$0.73 \pm 0.04 \pm 0.04$	$0.71 \pm 0.04^{+0.05}_{-0.04}$	$0.621^{+0.040+0.040}_{-0.035-0.035}$
purity	$0.209^{+0.014+0.012}_{-0.012-0.012}$	$0.218^{+0.014+0.032}_{-0.013-0.030}$	$0.259^{+0.015+0.012}_{-0.014-0.012}$

TABLE III. Thermal occupancies of the X and Y modes considered as one-dimensional oscillators, and two-dimensional state purity deduced for the three different data sets. The first reported uncertainty is derived from the statistical spread of the fitted parameters, the second quoted error derives from a spread of 5% in the detection efficiency.